Editors' Suggestion

Spin-density wave of ferrimagnetic building blocks masking the ferromagnetic quantum critical point in $NbFe_2$

T. Poulis [1,*] G. Mani [1] J. Sturt [1] W. J. Duncan,[1] H. Thoma [2,3] V. Hutanu [2,3] B. Ouladdiaf [4] I. Kibalin [4] M. H. Lemee,[4] P. Manuel,[5] A. Neubauer [6] C. Pfleiderer [6] F. M. Grosche [7] and P. G. Niklowitz [1,†]

[1]*Department of Physics, Royal Holloway, University of London, Egham TW20 0EX, United Kingdom*
[2]*Institute of Crystallography, RWTH Aachen University, 52066 Aachen, Germany*
[3]*Jülich Centre for Neutron Science (JCNS) at Heinz Maier-Leibnitz Zentrum (MLZ), D-85747 Garching, Germany*
[4]*Institut Laue Langevin, 38042 Grenoble Cedex 9, France*
[5]*ISIS Neutron and Muon Source, STFC Rutherford Appleton Laboratory, Didcot OX11 0QX, United Kingdom*
[6]*Physik Department E21, Technische Universität München, 85748 Garching, Germany*
[7]*Cavendish Laboratory, University of Cambridge, Cambridge CB3 0HE, United Kingdom*

(Received 31 December 2025; revised 4 August 2026; accepted 4 August 2026; published 5 October 2026)

In the metallic magnet $NbFe_2$, the low temperature threshold of ferromagnetism can be investigated by varying the Fe concentration within a narrow homogeneity range. $NbFe_2$ is one of a number of compounds where modulated order is found to mask the ferromagnetic quantum critical point. However, here we report the rare case where the masking modulated magnetic order has been fully refined. Spherical neutron polarimetry and high-intensity single-crystal neutron diffraction reveal the first case of a longitudinal spin-density wave masking the ferromagnetic quantum critical point. The spin-density wave is characterized by a large-wavelength incommensurate modulation of its low average moment. It is formed from ferrimagnetic building blocks with antiparallel ferromagnetic sheets. The existence of ferromagnetic sheets and compensation of the magnetization only over mesoscopic length scales show local similarity between the spin-density wave and the ferromagnetic parent phase and indicate the spin-density wave's unconventional nature as emerging from underlying ferromagnetic quantum criticality.

DOI: 10.1103/lcrw-ptwv

I. INTRODUCTION

The exploration of ferromagnetic (FM) quantum phase transitions in metals has motivated numerous theoretical and experimental studies [1], which have led to the discovery of non-Fermi liquid states [2,3] and of unconventional superconductivity (e.g., Refs. [4–6]). The underlying question, however, whether an FM quantum critical point (QCP) can exist in clean band magnets, remains controversial. Fundamental considerations [7–9] suggest that the FM QCP is avoided in clean systems by one of two scenarios: either the transition into the FM state becomes discontinuous (first order), or the nature of the low temperature ordered state changes altogether, for instance into nematic or long-wavelength spin density wave (SDW) order [8,9]. Examples for the first scenario, include $ZrZn_2$ [2,10], Ni_3Al [3] and UGe_2 [4,11]. Examples for the transition into a modulated state include: (i) the masking of the field-tuned quantum-critical end point of the continuous metamagnetic transition of $Sr_3Ru_2O_7$ by two SDW orders [12] with enhanced spin fluctuations in the ordered states [13] and the field-induced suppression of FM and replacement with a modulated fan state in the local moment system PrPtAl [14,15], (ii) modulated order in the heavy-fermion system $YbRh_2Si_2$ that is adjacent to FM under Co doping [16,17], features a high Wilson ratio [18] and the evolution of FM fluctuations into long-wavelength SDW fluctuations upon cooling [19] and hosts a candidate for odd-parity superconductivity boosted by an electronuclear SDW [20–22], (iii) and at the border of pressure-tuned FM the appearance of modulated magnetic order in CeRuPO [23] and helical magnetic order terminating in superconductivity in MnP [24–27], while pressure-induced short-range FM clusters are reported at the border of long-range FM in $LaCrGe_3$ [28,29].

An incommensurate SDW masking the border of itinerant FM at zero temperature, field, and pressure is found in $Nb_{1-y}Fe_{2+y}$. The border of FM is located near stoichiometric $NbFe_2$ [32], where it is masked by modulated order. FM order can be induced at low temperature by growing Fe-rich $Nb_{1-y}Fe_{2+y}$ with y as small as 1% (Fig. 1 [31]). The SDW nature of the modulated order at the border of FM was indicated by nuclear magnetic resonance [33], electron spin resonance, muon spin resonance (μSR), and Mößbauer spectroscopy [34]. Neutron scattering revealed a long-wavelength SDW with associated ordering wave vector $\mathbf{q}_{\mathrm{SDW}} = (0, 0, l_{\mathrm{SDW}})$. l_{SDW} is of the order 0.1 r.l.u but found to depend substantially on y and T, decreasing as the FM state is approached

*Contact author: thomas.poulis.2022@live.rhul.ac.uk
†Contact author: philipp.niklowitz@rhul.ac.uk

Published by the American Physical Society under the terms of the Creative Commons Attribution 4.0 International license. Further distribution of this work must maintain attribution to the author(s) and the published article's title, journal citation, and DOI.

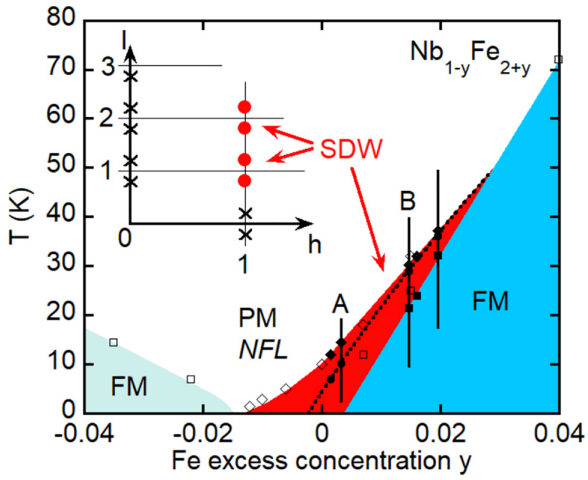


FIG. 1. Phase diagram of $Nb_{1-y}Fe_{2+y}$ with results for bulk T_C (squares) and T_N (diamonds) from previous single-crystal (filled symbols) [30] and polycrystal (empty symbols) [31] studies. Vertical solid lines indicate the T range of previous cold neutron diffraction measurements. A and B denote samples also studied with thermal neutron diffraction reported here. Of the two ferromagnetic (FM) phases, the one on the more Fe-rich side is separated from the paramagnetic (PM) state by a /SDW at low temperatures, where NFL behavior is found as well. T_0, the FM phase boundary buried by the SDW phase (dashed line) is an extrapolation of T_0 values (circles) measured or calculated for the single crystals. The inset shows the relevant reciprocal-space region, which was accessible during previous neutron diffraction experiments. Circles show the presence and crosses the absence of SDW peaks.

but staying finite at the first-order SDW-FM phase transition [30]. Non-Fermi-liquid (NFL) forms of resistivity and low temperature heat capacity have been observed in slightly Nb-rich $NbFe_2$ in the vicinity of the SDW phase [35]. The SDW's structure factor and therefore its microscopic details within the $NbFe_2$ unit cell including the effective moment size and orientation at the individual magnetic sites have been unknown so far.

Here we present the full magnetic structure of the spin-density-wave phase. Spherical neutron polarimetry (SNP) excluded spiral order and transverse SDW order as reported for other compounds [12,14]. High-intensity single-crystal neutron diffraction (ND) in particular has allowed full refinement despite a low average moment of 0.039 μ_B/atom. A longitudinal spin-density wave with a large-wavelength incommensurate modulation along the magnetic easy *c*axis is formed from ferrimagnetic unit-cell building blocks with antiparallel ferromagnetic sheets stacked along the *c*axis. In particular, this excludes the possibility of a compensation of the magnetization within the $NbFe_2$ unit cell. The compensation of the magnetization only over length scales of 50–90 Å indicates the spin-density wave's unconventional nature as emerging from underlying ferromagnetic quantum criticality.

II. EXPERIMENTAL DETAILS

Large single crystals of C14 Laves phase $NbFe_2$ (lattice constants $a \approx 4.84$ Å and $c \approx 7.89$ Å) with compositions chosen across the iron-rich side of the homogeneity range have been grown in a UHV-compatible optical floating zone furnace from polycrystals prepared by induction melting [36]. The single crystals have been characterized extensively by resistivity, susceptibility, and magnetization measurements, as well as by x-ray diffraction and neutron depolarization [37–39], the latter showing homogeneity in structure and chemical composition.

Here, two samples that were already used to measure the SDW ordering wave vector [30] have been studied: (i) sample A is almost stoichiometric ($y = +0.003$) with T_N at 15.3 K (revisited from the value reported in Ref. [30] based on more detailed low-T measurements as described in Supplemental Material [40]) and an SDW ordering vector q_{SDW} =(0 0 0.156); (ii) sample B is slightly Fe rich ($y = +0.015$) with T_N and T_C at 32.5 K and 19 K, respectively, and q_{SDW} =(0 0 0.10).

The set of polycrystals and single crystals (including the samples of this study) [31,39] on which the phase diagram in Fig. 1 is based have residual resistivities in the range of 5–19 μΩ cm. According to theoretical studies of the disorder dependence of FM quantum phase transitions [41,42] this would place them at the lower end of the intermediate regime (several to hundreds of μΩ cm) for which a FM QCP is predicted. However, those predictions are rough order-of-magnitude estimates, which means that the observation of the the phase diagram in Fig. 1 that matches the prediction for the clean limit does not represent a clear contradiction with theory.

For the neutron scattering experiments the samples were mounted on Al holders. The nature of magnetic order was determined with SNP using Cryopad at the polarized hot neutron diffractometer POLI (MLZ) [43,44]. The beamline set-up included polarized ^{3}He spin filters as both polarizers and analyzers, and a Cu crystal monochromator set to select a neutron wavelength of $\lambda = 0.9$ Å. The sample was mounted on a standard closed-cycle cryostat.

The full magnetic structure was obtained through unpolarized single-crystal ND at four-circle diffractometer D10+ (ILL) [45]. The monochromator was set to $\lambda = 2.363$ Å. A pyrolytic graphite filter suppressed higher-order harmonics. An analyzer to reduce the quasielastic background was essential to detect the SDW Bragg peak signals that were collected with a single-counter ^{3}He detector. The sample was cooled with a Joule-Thomson displex. A few magnetic peaks have additionally been measured with time-of-flight spectrometer WISH at ISIS [40].

III. RESULTS

SNP was done on slightly Fe-rich Sample B at $T = 25$ K in the SDW state. Background measurements at $T = 50$ K confirmed the paramagnetic (PM) phase. The full set of 36 channels was obtained at the two strong magnetic Bragg peaks, $Q = (2\bar{2}1.1)$ and $Q = (2\bar{2}3.1)$. Scattering factors at 25 K have been obtained from two independent analysis methods: a numerical method (Table I) and an analytical method (see Supplemental Material [40]), which agree within the error.

The scattering factors in Table I reveal that the SDW phase is formed by collinear magnetic moments along the easy

TABLE I. Scattering factors of nuclear (N) and magnetic (M) scattering obtained from least-squares fitting of the results at 25 K for all 36 SNP channels. The coordinates are defined as $x \| \mathbf{Q}$, $y \perp x$ and in the ($h0l$) scattering plane, and $z \perp x, y$.

Scattering factors	Q = $(2\overline{21.1})$	Q = $(22\overline{3.1})$
NN^*	0.025 ± 0.011	0.002 ± 0.000
$M_yM_y^*$	7.559 ± 0.455	2.450 ± 0.176
$M_zM_z^*$	0.019 ± 0.018	0.014 ± 0.014
$i(M_\perp \times M_\perp^*)$	-0.340 ± 0.020	0.090 ± 0.100
$Re(M_yM_z^*)$	-0.150 ± 0.300	-0.140 ± 0.109
$Re(NM_y^*)$	0.299 ± 0.139	0.014 ± 0.039
$Re(NM_z^*)$	-0.003 ± 0.019	-0.003 ± 0.006
$Im(NM_y^*)$	-0.250 ± 0.025	0.150 ± 0.099
$Im(NM_z^*)$	0.014 ± 0.016	-0.013 ± 0.013

c axis. The only positive signals substantially larger than the error range at both investigated magnetic Bragg peaks are found for $M_yM_y^*$. In particular, the $M_zM_z^*$ signal of z components in the hexagonal ab plane (Table I) is within the noise. Given the hexagonal symmetry of the $Nb_{1-y}Fe_{2+y}$ crystal structure, magnetic order is often expected to preserve or respect the abplane symmetry. A zero $M_zM_z^*$ signal is only possible if the SDW moments have their spins predominantly oriented on the c axis. This and the previously reported ordering wave vector $\mathbf{q}_{SDW} = (0, 0, l_{SDW})$ [30] means that the SDW in $Nb_{1-y}Fe_{2+y}$ is longitudinal. This conclusion is also in agreement with the previously reported absence of magnetic diffraction peaks at $\mathbf{q} = (00l \pm l_{SDW})$ with $l = 1, 2, 3$ [30] when taking into account the relevant neutron selection rule.

Candidates for the SDW's irreducible representations were identified with the SARAh Refine program [46] based on the $NbFe_2$ crystal structure and its SDW propagation vector. Four possible irreducible representations were found for the Fe_{2a} site, six for Fe_{6h}, and the same four as for Fe_{2a} for each of the two Nb sites that separate into two distinct magnetic sites (Nb_1 and Nb_2) within the $P6_3/mmc$ space group. Two further constraints are: (i) the SNP result described above that the SDW is formed of magnetic moments along the c axis, and (ii) the SDW phase is separated from PM by a single critical temperature, which points to a single common irreducible representation for all magnetic sites [47]. Only two such representations out of the six satisfy these further constraints: one candidate is the Γ_2 representation where the magnetic moments on symmetry-equivalent sites are ferromagnetically aligned. The other candidate is Γ_4 with antiferromagnetic alignment between symmetry-equivalent sites. Both representations include, for the Fe atoms on the 6h Wyckoff position the potential for in-plane (ab) components. These in-plane components would cause three Fe atoms of kagome triangle to orient in all-in or all-out configurations. Those do not contribute to the unit-cell's net magnetization, which for Γ_2 and Γ_4 can therefore only be collinear with the easy c axis.

Unpolarized ND was collected on almost stoichiometric ($y = +0.003$) Sample A at a $T = 4$ K in the SDW state. SDW peaks at 104 different positions falling into 23 sets of symmetrically independent reflections were measured to enable full structure refinement. The magnetic peaks were fitted with

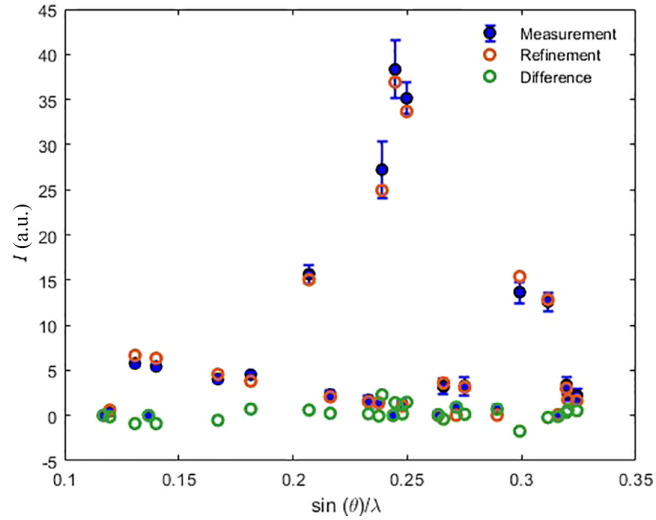


FIG. 2. Refinement of SDW Bragg peaks from unpolarized ND by the Γ_2 representation that leads to the best agreement (see fit parameters in Table II).

Gaussian functions. Magnetic intensities were corrected for two effects (see Supplemental Material [40]): (i) amplitude reduction of strong nuclear peaks by detector saturation and (ii) a single-counter-detector induced reduction of the peak width beyond the q dependent instrument resolution.

Corrected SDW peak intensities were used for structural refinement with FullProf. The Γ_2 representation that meets all constraints discussed above from crystal symmetry, SNP results and the phase diagram can be brought into excellent agreement with the data, as shown in Fig. 2. All basis vectors permitted by the Γ_2 representation were refined simultaneously and the goodness of fit parameters are presented in Table II. Despite the relatively weak magnetic intensities and moments, refinement results with R values $<15\%$ are quite robust. Figure 3 depicts the magnetic-moment arrangement in a crystal-lattice unit cell that acts as a building block for the

TABLE II. Refined amplitudes of the spin-density-wave (SDW) magnetic moments (in μ_B) along the crystallographic a, b, and c axes. The amplitude of the net unit-cell magnetic moment is $m_{amp} = \frac{1}{n}|\sum_{i=1}^{n} S_i|$. The average magnitude of the net unit-cell magnetic moment is $\bar{m}_{av} = \frac{1}{n N_{cell}} \sum_{\ell=1}^{N_{cell}} |\sum_{j=1}^{n} S_j|$. Uncertainties reflect the propagation of errors from the FullProf basis-vector refinements. Goodness-of-fit parameters are listed below.

Site	S_a (μ_B)	S_b (μ_B)	S_c (μ_B)
Fe_{2a}	0	0	0.0439 ± 0.0021
Fe_{6h}	0	0	-0.0849 ± 0.0016
Nb_1	0	0	-0.0135 ± 0.0202
Nb_2	0	0	-0.0097 ± 0.0066
m_{amp} (μ_B/atom)	0.0390 ± 0.0062		
$\bar{m}_{av}$ (μ_B/atom)	0.0249 ± 0.0062		
R_{F^2}	8.306		
R_{F^2w}	13.11		
R_F	8.875		
χ^2	1.583		

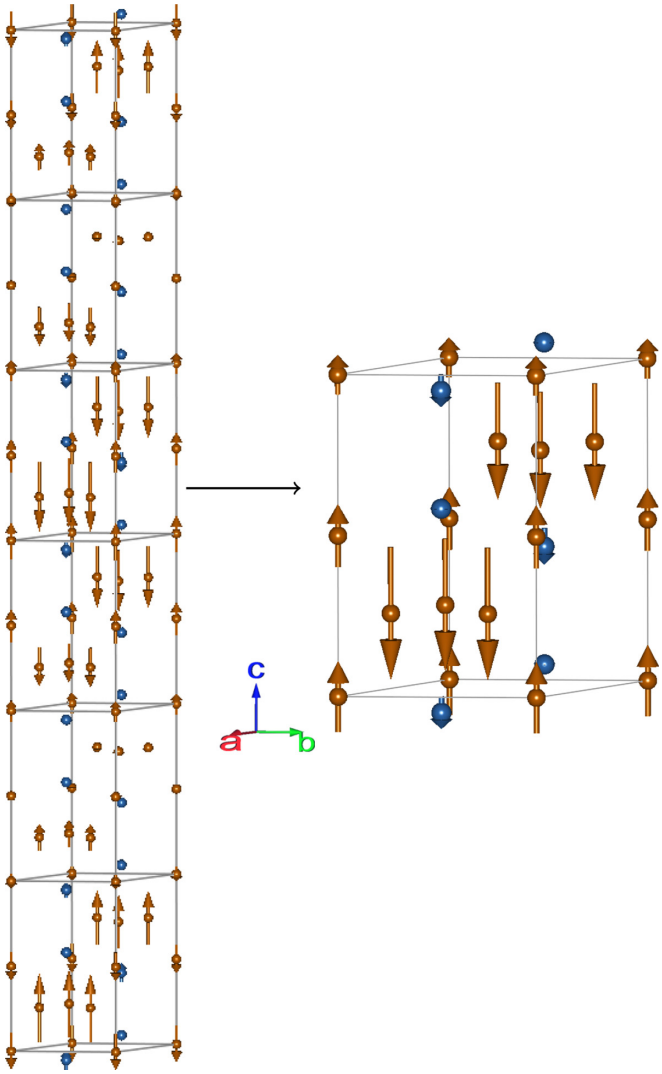


FIG. 3. Six-unit-cell SDW structure with highlighted region (left) and zoomed-in single-unit-cell model (right), including Cartesian axes, of the ferrimagnetic building block of the incommensurate long-wavelength SDW structure of $NbFe_2$ from refinement of unpolarized ND data. Fe atoms (orange) and Nb atoms (blue) each form ferrimagnetic sublattices.

SDW structure with its longer-range incommensurate modulation. Within such a building block the Γ_2 representation is characterized by parallel arrangement of magnetic moments at a given type of magnetic site. This creates ferromagnetic layers parallel to the *ab* plane. Neighboring Fe layers are aligned antiparallel with different moment sizes, creating a ferrimagnetic arrangement within the building block. The Nb sublattice also carries magnetic order with the net moment pointing in the same direction as the net moment of the Fe lattice. Models based on other representations including those where moments exclusively have *ab* plane components were also tested. None provided a satisfactory fit to the data, with refinement of Γ_4 as the next best representation leading to at least an order of magnitude larger goodness-of-fit values.

IV. DISCUSSION

The magnetic-moment amplitudes obtained from the refinement of unpolarised ND intensities (Table II) result in an amplitude of the net unit-cell magnetic moment of $m_{\text{amp}} = \frac{1}{n}|\sum_{i=1}^{n} S_i| = 0.0390 \pm 0.0062\ \mu_B$/atom where n is the number of atoms. Due to the long-range modulation of the unit-cell structure the average magnitude of the net unit-cell magnetic moment is $\bar{m}_{\text{av}} = \frac{1}{n N_{\text{cell}}} \sum_{\ell=1}^{N_{\text{cell}}} |\sum_{j=1}^{n} S_j| = 0.0249 \pm 0.0062\ \mu_B$/atom, where S_i is the magnetic moment of the spin i, n is the number of atoms in a unit cell, and N_{cell} is the number of unit cells, in excellent agreement with μSR measurements [48] that reported 0.03 μ_B per Fe atom. The minimal size of magnetic-moment components in the *ab* plane agrees with the SNP results reported above.

The presence of FM sheets in the *ab* plane has also been seen in $TiFe_2$ [49]. This is another Laves phase compound whose magnetic order is sensitive to stoichiometry, with the bulk of the magnetic moments parallel to the *c* axis and concentrated on the Fe_{6h} iron sheets, which are coupled ferromagnetically. However, in contrast to $TiFe_2$, for $NbFe_2$, the assumption of no magnetic moments on the Fe_{2a} sites leads to poor refinement of the ND data although the magnetic moments on those sites in $NbFe_2$ are very small. For other Laves phase compounds, their absence has been related to topological frustration [49] although the role of frustration in itinerant magnets tends to be reduced.

A main consequence of the emergence of the longitudinal incommensurate SDW in $NbFe_2$ is that the formation of the FM QCP is prevented. To the authors' knowledge, this is the first observation of a longitudinal SDW emerging from the border of FM, but fanlike SDW order is reported to mask a magnetic-field tuned QCP in PrPtAl [15] and transverse SDW order is reported to mask a magnetic-field tuned metamagnetic quantum-critical endpoint in $Sr_3Ru_2O_7$ [12]. Furthermore, helical magnetic order appears to mask a FM QCP in MnP under pressure [25–27]. These examples support theories that predict the intrinsic instability of QCPs in clean ferromagnets and their replacement by modulated magnetic phases [8,9,50]. The latter phases are stabilized by offering increased phase space for electronic low-energy particle-hole excitations, a mechanism known as quantum order by disorder [51,52]. $NbFe_2$ as a band magnet hosting this scenario at zero field will allow to test those theories in their most basic form.

The ferrimagnetic stacking of FM layers along the *c*axis means that there is a finite net magnetization within the crystal-lattice unit-cell building block, in contrast to, e.g., antiferromagnetic stacking. The local finite net magnetization in $NbFe_2$ is therefore only compensated over the mesoscopic length scales of the incommensurate SDW modulation of 50–90 Å and the SDW mimics FM at microscopic length scales. Similar length scales for magnetization compensation are observed for for the modulated component in PrPtAl (∼30 Å), for $Sr_3Ru_2O_7$ (∼25 Å) and for MnP (∼15 Å), which suggests that this could be a generic feature of modulated order emerging at the border of FM.

The ferrimagnetic moment configuration in the SDW building blocks suggests that the magnetic parent phase of $NbFe_2$ is not FM, but ferrimagnetic as well. Density

functional theory studies have suggested ferrimagnetism as a possible ground state of $NbFe_2$ among a number of candidate magnetic ground states with very small energy differences between them [53–55]. The calculations overestimate the magnetic site moment magnitudes, as is often the case for systems with enhanced magnetic fluctuations. Compton scattering results on the Fe-rich side of the phase diagram have also been analyzed by assuming ferrimagnetism as the ground state [56]. Because of the location of the stopping site, μSR data [48] could not distinguish between FM and ferrimagnetic order. Mößbauer results have been interpreted as indication of FM order [34].

If one assumed ferrimagnetic order for the parent phase, it would be intuitive to imagine it to simply be the SDW order without the long-wavelength modulation, which would have a net magnetization of approximately 0.0390 μ_B/atom. If one assumes FM order for the parent state, the natural guess would be a parallel alignment of all moments listed in Table II. This results in an average magnetization of 0.0536 μ_B/atom. Magnetization measurements in the parent phase in Fe-rich samples phase [57] detect an average magnetization of approximately 0.06 μ_B per atom. While this comparison leans more to the parent phase being ferromagnetic, a conclusive answer will likely require a direct observation of the magnetic parent-phase structure by polarized neutron diffraction.

V. CONCLUSION

This work shows that the emerging modulated structure of the itinerant ferromagnet $NbFe_2$ is an incommensurate long-wavelength SDW formed from ferrimagnetic blocks of FM planes stacked along the easy c axis. The existence of ferromagnetic sheets and compensation of the magnetization only over substantial length scales indicates the spin-density wave's unconventional nature as emerging from underlying ferromagnetic quantum criticality.

ACKNOWLEDGMENTS

This work is based upon experiments performed at D10+ of Institut Laue-Langevin (ILL), Grenoble, France [45] and at the POLI instrument operated by JCNS/ Forschungszentrum Jülich GmbH and RWTH Aachen University at the Heinz Maier-Leibnitz Zentrum (MLZ), Garching, Germany [43,44]. Further experiments at the WISH beamline of the ISIS Neutron and Muon Source were supported by beamtime allocation from the Science and Technology Facilities Council [58]. The instrument POLI [43] received funding from the German Federal Ministry of Research, Technology and Space (BMFTR, formerly BMBF) in the framework of the ErUM-Pro programme (Grants No. 05K10PA2 and No. 05K13PA3). The authors gratefully acknowledge the financial support provided by the ILL to perform the neutron scattering measurements there and by JCNS/ Forschungszentrum Jülich GmbH to perform the neutron scattering measurements at MLZ. The authors acknowledge support by the EPSRC through Grant No. EP/K012894/1. The authors thank D. Voneshen for assistance with Mantid Project software and N. A. Katcho and E. Canonero for helpful discussions.

DATA AVAILABILITY

The data that support the findings of this article are openly available [44,45,58].

[1] M. Brando, D. Belitz, F. M. Grosche, and T. R. Kirkpatrick, Metallic quantum ferromagnets, Rev. Mod. Phys. **88**, 025006 (2016).

[2] M. Uhlarz, C. Pfleiderer, and S. M. Hayden, Quantum Phase Transitions in the Itinerant Ferromagnet $ZrZn_2$, Phys. Rev. Lett. **93**, 256404 (2004).

[3] P. G. Niklowitz, F. Beckers, G. G. Lonzarich, G. Knebel, B. Salce, J. Thomasson, N. Bernhoeft, D. Braithwaite, and J. Flouquet, Spin-fluctuation-dominated electrical transport of Ni_3Al at high pressure, Phys. Rev. B **72**, 024424 (2005).

[4] C. Pfleiderer and A. D. Huxley, Pressure dependence of the magnetization in the ferromagnetic superconductor UGe_2, Phys. Rev. Lett. **89**, 147005 (2002).

[5] S. S. Saxena, P. Agarwal, K. Ahilan, F. M. Grosche, R. K. W. Haselwimmer, M. J. Steiner, E. Pugh, I. R. Walker, S. R. Julian, P. Monthoux, G. G. Lonzarich, A. Huxley, I. Sheikin, D. Braithwaite, and J. Flouquet, Superconductivity on the border of itinerant-electron ferromagnetism in UGe2, Nature (London) **406**, 587 (2000).

[6] P. L. Alireza, F. Nakamura, S. K. Goh, Y. Maeno, S. Nakatsuji, Y. T. C. Ko, M. Sutherland, S. Julian, and G. G. Lonzarich, Evidence of superconductivity on the border of quasi-2D ferromagnetism in Ca_2RuO_4 at high pressure, J. Phys.: Condens. Matter **22**, 052202 (2010).

[7] C. Pfleiderer, Superconducting phases of f-electron compounds, Rev. Mod. Phys. **81**, 1551 (2009).

[8] T. Vojta, D. Belitz, T. R. Kirkpatrick, and R. Narayanan, Quantum critical behavior of itinerant ferromagnets, Ann. Phys. (Leipzig) **511**, 593 (1999).

[9] A. V. Chubukov, C. Pepin, and J. Rech, Instability of the quantum-critical point of itinerant ferromagnets, Phys. Rev. Lett. **92**, 147003 (2004).

[10] N. Kabeya, H. Maekawa, K. Deguchi, N. Kimura, H. Aoki, and N. K. Sato, Phase diagram of the itinerant-electron ferromagnet $ZrZn_2$, Phys. Status Solidi B **250**, 654 (2013).

[11] V. Taufour, D. Aoki, G. Knebel, and J. Flouquet, Tricritical point and wing structure in the itinerant ferromagnet UGe_2, Phys. Rev. Lett. **105**, 217201 (2010).

[12] C. Lester, S. Ramos, R. S. Perry, T. P. Croft, R. I. Brewley, T. Guidi, P. Manuel, D. D. Khalyavin, E. M. Forgan, and S. M. Hayden, Field-tunable spin-density-wave phases in $Sr_3Ru_2O_7$, Nat. Mater. **14**, 373 (2015).

[13] C. Lester, S. Ramos, R. S. Perry, T. P. Croft, M. Laver, R. I. Brewley, T. Guidi, A. Hiess, A. Wildes, E. M. Forgan, and S. M. Hayden, Magnetic-field-controlled spin fluctuations and quantum criticality in $Sr_3Ru_2O_7$, Nat. Commun. **12**, 5798 (2021).

[14] G. Abdul-Jabbar, D. A. Sokolov, C. D. O'Neill, C. Stock, D. Wermeille, F. Demmel, F. Krüger, A. G. Green,

F. Lévy-Bertrand, B. Grenier, and A. D. Huxley, Modulated magnetism in PrPtAl, Nat. Phys. **11**, 321 (2015).
[15] C. D. O'Neill, G. Abdul-Jabbar, D. Wermeille, P. Bourges, F. Krüger, and A. D. Huxley, Field-induced modulated state in the ferromagnet PrPtAl, Phys. Rev. Lett. **126**, 197203 (2021).
[16] S. Lausberg, A. Hannaske, A. Steppke, L. Steinke, T. Gruner, L. Pedrero, C. Krellner, C. Klingner, M. Brando, C. Geibel, and F. Steglich, Doped $YbRh_2Si_2$: Not only ferromagnetic correlations but ferromagnetic order, Phys. Rev. Lett. **110**, 256402 (2013).
[17] S. Hamann, J. Zhang, D. Jang, A. Hannaske, L. Steinke, S. Lausberg, L. Pedrero, C. Klingner, M. Baenitz, F. Steglich, C. Krellner, C. Geibel, and M. Brando, Evolution from ferromagnetism to antiferromagnetism in $Yb(Rh_{1-x}Co_x)_2Si_2$, Phys. Rev. Lett. **122**, 077202 (2019).
[18] P. Gegenwart, J. Custers, Y. Tokiwa, C. Geibel, and F. Steglich, Ferromagnetic quantum critical fluctuations in $YbRh_2(Si_{0.95}Ge_{0.05})_2$, Phys. Rev. Lett. **94**, 076402 (2005).
[19] C. Stock, C. Broholm, F. Demmel, J. Van Duijn, J. W. Taylor, H. J. Kang, R. Hu, and C. Petrovic, From incommensurate correlations to mesoscopic spin resonance in $YbRh_2Si_2$, Phys. Rev. Lett. **109**, 127201 (2012).
[20] E. Schuberth, M. Tippmann, L. Steinke, S. Lausberg, A. Steppke, M. Brando, C. Krellner, C. Geibel, R. Yu, Q. Si, and F. Steglich, Emergence of superconductivity in the canonical heavy-electron metal $YbRh_2Si_2$, Science **351**, 485 (2016).
[21] D. H. Nguyen, A. Sidorenko, M. Taupin, G. Knebel, G. Lapertot, E. Schuberth, and S. Paschen, Superconductivity in an extreme strange metal, Nat. Commun. **12**, 4341 (2021).
[22] L. V. Levitin, J. Knapp, P. Knappová, M. Lucas, J. Nyéki, P. Heikkinen, V. Antonov, A. Casey, A. F. Ho, P. Coleman, C. Geibel, A. Steppke, K. Kliemt, C. Krellner, M. Brando, and J. Saunders, Evidence for odd-parity superconductivity underpinned by antiferromagnetism in heavy-fermion metal $YbRh_2Si_2$, Nat. Phys. **22**, 713 (2026).
[23] E. Lengyel, M. E. Macovei, A. Jesche, C. Krellner, C. Geibel, and M. Nicklas, Avoided ferromagnetic quantum critical point in CeRuPO, Phys. Rev. B **91**, 035130 (2015).
[24] J.-G. Cheng, K. Matsubayashi, W. Wu, J. P. Sun, F. K. Lin, J. L. Luo, and Y. Uwatoko, Pressure induced superconductivity on the border of magnetic order in MnP, Phys. Rev. Lett. **114**, 117001 (2015).
[25] M. Matsuda, F. Ye, S. E. Dissanayake, J.-G. Cheng, S. Chi, J. Ma, H. D. Zhou, J.-Q. Yan, S. Kasamatsu, O. Sugino, T. Kato, K. Matsubayashi, T. Okada, and Y. Uwatoko, Pressure dependence of the magnetic ground states in MnP, Phys. Rev. B **93**, 100405(R) (2016).
[26] R. Khasanov, A. Amato, P. Bonfà, Z. Guguchia, H. Luetkens, E. Morenzoni, R. Derenzi, and N. D. Zhigadlo, High-pressure magnetic state of MnP probed by means of muon-spin rotation, Phys. Rev. B **93**, 180509(R) (2016).
[27] S. E. Dissanayake, M. Matsuda, K. Yoshimi, S. Kasamatsu, F. Ye, S. Chi, W. Steinhardt, G. Fabbris, S. Haravifard, J. Cheng, J. Yan, J. Gouchi, and Y. Uwatoko, Helical magnetic state in the vicinity of the pressure-induced superconducting phase in MnP, Phys. Rev. Res. **5**, 043026 (2023).
[28] U. S. Kaluarachchi, S. L. Bud'ko, P. C. Canfield, and V. Taufour, Tricritical wings and modulated magnetic phases in $LaCrGe_3$ under pressure, Nat. Commun. **8**, 546 (2017).
[29] E. Gati, J. M. Wilde, R. Khasanov, L. Xiang, S. Dissanayake, R. Gupta, M. Matsuda, F. Ye, B. Haberl, U. Kaluarachchi, *et al.*, Formation of short-range magnetic order and avoided ferromagnetic quantum criticality in pressurized $LaCrGe_3$, Phys. Rev. B **103**, 075111 (2021).
[30] P. G. Niklowitz, M. Hirschberger, M. Lucas, P. Cermak, A. Schneidewind, E. Faulhaber, J.-M. Mignot, W. J. Duncan, A. Neubauer, C. Pfleiderer, and F. M. Grosche, Ultrasmall moment incommensurate spin density wave order masking a ferromagnetic quantum critical point in $NbFe_2$, Phys. Rev. Lett. **123**, 247203 (2019).
[31] D. Moroni-Klementowicz, M. Brando, C. Albrecht, W. J. Duncan, F. M. Grosche, D. Grüner, and G. Kreiner, Magnetism in $Nb_{1-y}Fe_{2+y}$: Composition and magnetic field dependence, Phys. Rev. B **79**, 224410 (2009).
[32] M. Shiga and Y. Nakamura, Magnetic Properties of Stoichiometric and Off-Stoichiometric $NbFe_2$, J. Phys. Soc. Jpn. **56**, 4040 (1987).
[33] Y. Yamada and A. Sakata, Weak Antiferromagnetism in $NbFe_2$, J. Phys. Soc. Jpn. **57**, 46 (1988).
[34] D. Rauch, M. Kraken, F. J. Litterst, S. Süllow, H. Luetkens, M. Brando, T. Förster, J. Sichelschmidt, A. Neubauer, C. Pfleiderer, W. J. Duncan, and F. M. Grosche, Spectroscopic study of metallic magnetism in single-crystalline $Nb_{1-y}Fe_{2+y}$, Phys. Rev. B **91**, 174404 (2015).
[35] M. Brando, W. J. Duncan, D. Moroni-Klementowicz, C. Albrecht, D. Grüner, R. Ballou, and F. M. Grosche, Logarithmic fermi-liquid breakdown in $NbFe_2$, Phys. Rev. Lett. **101**, 026401 (2008).
[36] A. Neubauer, J. Boeuf, A. Bauer, B. Russ, H. v. Löhneysen, and C. Pfleiderer, Ultra-high vacuum compatible image furnace, Rev. Sci. Instrum. **82**, 013902 (2011).
[37] C. Pfleiderer, P. Böni, C. Franz, T. Keller, A. Neubauer, P. G. Niklowitz, P. Schmakat, M. Schulz, Y. K. Huang, J. A. Mydosh, M. Vojta, W. Duncan, F. M. Grosche, M. Brando, M. Deppe, C. Geibel, F. Steglich, A. Krimmel, and A. Loidl, Search for electronic phase separation at quantum phase transitions, J. Low Temp. Phys. **161**, 167 (2010).
[38] A. Neubauer, Ph.D. thesis, Technische Universität München, 2011.
[39] W. Duncan, Ph.D. thesis, Royal Holloway, University of London, 2011.
[40] See Supplemental Material at http://link.aps.org/supplemental/10.1103/lcrw-ptwv for more details on experimental details, data fitting and data analysis, which also includes Refs. [59–64].
[41] D. Belitz, T. R. Kirkpatrick, and T. Vojta, First order transitions and multicritical points in weak itinerant ferromagnets, Phys. Rev. Lett. **82**, 4707 (1999).
[42] Y. Sang, D. Belitz, and T. R. Kirkpatrick, Disorder dependence of the ferromagnetic quantum phase transition, Phys. Rev. Lett. **113**, 207201 (2014).
[43] V. Hutanu, Heinz Maier-Leibnitz Zentrum, POLI: Polarised hot neutron diffractometer, J. Large-Scale Res. Facil. **1**, A16 (2015).
[44] P. Niklowitz, POLI, MLZ neutron data from June 2018, beamtime proposal number p14147, Royal Holloway, University of London, Dataset, 2026, https://doi.org/10.17637/rh.30979666.
[45] P. G. Niklowitz, T. Poulis, B. Ouladdiaf, I. Kibalin, M. H. Lemee, and N. A. Katcho, Magnetic structure of the emerging spin density wave phase in Nb1-yFe2+y, Institut Laue-Langevin (ILL) (2023), https://doi.ill.fr/10.5291/ILL-DATA.5-41-1192.

[46] A. S. Wills, A new protocol for the determination of magnetic structures using simulated annealing and representational analysis (SARAh), Physica B **276-278**, 680 (2000).

[47] A. Wills, Magnetic structures and their determination using group theory, J. Phys. IV France **11**, 133 (2001).

[48] J. Willwater, D. Eppers, T. Kimmel, E. Sadrollahi, F.J. Litterst, F.M. Grosche, C. Baines, and S. Sullow, Muon spin rotation and relaxation study on $Nb_{1-y}Fe_{2+y}$, Phys. Rev. B **106**, 134408 (2022).

[49] P. Brown, J. Deportes, and B. Ouladdiaf, Magnetic structure of the Laves phase compound $TiFe_2$, J. Phys.: Condens. Matter **4**, 10015 (1992).

[50] D. Belitz, T. R. Kirkpatrick, and T. Vojta, Nonanalytic behavior of the spin susceptibility in clean Fermi systems, Phys. Rev. B **55**, 9452 (1997).

[51] U. Karahasanovic, F. Krüger, and A. G. Green, Quantum order-by-disorder driven phase reconstruction in the vicinity of ferromagnetic quantum critical points, Phys. Rev. B **85**, 165111 (2012).

[52] A. G. Green, G. Conduit, and F. Krüger, Quantum order-by-disorder in strongly correlated metals, Annu. Rev. Condens. Matter Phys. **9**, 59 (2018).

[53] A. Subedi and D. J. Singh, Band structure and itinerant magnetism in quantum critical $NbFe_2$, Phys. Rev. B **81**, 024422 (2010).

[54] D. A. Tompsett, R. J. Needs, F. M. Grosche, and G. G. Lonzarich, Doping-driven magnetic instabilities and quantum criticality of $NbFe_2$, Phys. Rev. B **82**, 155137 (2010).

[55] B. P. Neal, E. R. Ylvisaker, and W. E. Pickett, Quantum criticality in $NbFe_2$ induced by zero carrier velocity, Phys. Rev. B **84**, 085133 (2011).

[56] T. D. Haynes, I. Maskery, M. W. Butchers, J. A. Duffy, J. W. Taylor, S. R. Giblin, C. Utfeld, J. Laverock, S. B. Dugdale, Y. Sakurai, M. Itou, C. Pfleiderer, M. Hirschberger, A. Neubauer, W. Duncan, and F. M. Grosche, Ferrimagnetism in Fe-rich $NbFe_2$, Phys. Rev. B **85**, 115137 (2012).

[57] S. Friedemann, M. Brando, W. J. Duncan, A. Neubauer, C. Pfleiderer, and F. M. Grosche, Ordinary and intrinsic anomalous Hall effects in $Nb_{1-y}Fe_{2+y}$, Phys. Rev. B **87**, 024410 (2013).

[58] P. G. Niklowitz, T. Poulis, and P. Manuel, Xpress measurement, STFC ISIS Neutron and Muon Source (2023), https://doi.org/10.5286/ISIS.E.RB0-17511.

[59] H. Thoma, V. Hutanu, SNP FileScanner - Tool for time dependent polarization corrections of polarized diffraction data, JCNS Workshop presentation, FZJ-2019-00329 (unpublished).

[60] M. Blume, Polarization effects in the magnetic elastic scattering of slow neutrons, Phys. Rev. **130**, 1670 (1963).

[61] O. Arnold, J.-C. Bilheux, J. Borreguero, A. Buts, S. I. Campbell, L. Chapon, M. Doucet, N. Draper, R. F. Leal, M. Gigg, *et al.*, Mantid—Data analysis and visualization package for neutron scattering and μSR experiments, Nucl. Instrum. Methods Phys. Res. Sect. A **764**, 156 (2014).

[62] R. B. Von Dreele, J. D. Jorgensen, and C. G. Windsor, Rietveld refinement with spallation neutron powder diffraction data, J. Appl. Crystallogr. **15**, 581 (1982).

[63] G. McIntyre and R. Stansfield, A general Lorentz correction for single-crystal diffractometers, Acta Crystallogr. Sect. A **44**, 257 (1988).

[64] J. Zhu, L. Pike, C. Liu, and P. Liaw, Point defects in binary Laves phase alloys, Acta Mater. **47**, 2003 (1999).